



Numerical Details of Convective Heat Transfer by Micro-Encapsulated PCM Case Study: Annular Slurry Flow

Javad Rostami*

Department of Mechanical Engineering, Faculty of Engineering, Razi University, P. Box: 6714414971, Kermanshah, Iran

Abstract

Due to the high latent heat value, using microencapsulated PCMs increases the heat transfer coefficient in the heat sinks in mini electronic devices, chilled ceiling, In this paper, convective heat transfer by mixed PCM particles in a fluid as slurry, has been studied by the Eulerian-Lagrangian two-phase method. In this method, the fluid phase is studied by the Eulerian and the particle phase is studied using the Lagrangian view. In this paper, the base fluid is water and the particles made of encapsulated micro-size paraffin wax which has covered by a thin layer of Fe_3O_4 . The fluid phase is solved by a control volume method (SIMPLE) and the velocities of the particle phase are solved by the 4th order of the Runge-Kutta method. Due to high Biot number for particles, the lumped temperature assumption for particles is not valid and the transient one dimensional conduction equation has been solved. In this paper details of solving the energy equation inside the particles has been presented. The results include the local and mean Nusselt numbers for different Reynolds numbers including 200, 350 and 500, wide range of the volume fraction from 0-5% for PCM particle with 10 micro-meter diameter, inside the mini annular tube with inner diameter of 1 mm and outer diameter of 3 mm. The results show for $\phi = 0.05$ and $Re=200, 500$, the Nusselt number increases by 10 and 12.5%, while the pressure loss increases by 2 and 5.5% respectively. The maximum performance coefficient is 1.078 and occurs for $Re=200$ at $\phi = 0.05$.

Keywords: Microcapsule, PCM, Eulerian-Lagrangian, Stephane number, Annular flow

Nomenclature

A_p	Particle area, m^2
Bi	Biot number
C_p	specific heat capacity, $J.kg^{-1}.K^{-1}$
C_D	Drag Force Coefficient
d_p, D_p	particle diameter, m
f	Friction factor
F	acting force on the particles, N
g	Gravity, $m.s^{-2}$
H	height of the mini-channel, m
h	Heat transfer coefficient $W.m^{-2}.K^{-1}$
h_p	Particle enthalpy $J.kg^{-1}$
k	thermal conductivity, $W.m^{-1}.K^{-1}$
L	channel length, m
L_0	Isotherm length, m

* Corresponding author: jrostami@razi.ac.ir

L_{sl}	Latent heat of the PCM, $J.kg^{-1}$
m	Mass, kg
N_p	Total particle number
n_p	particle number in a cell
n_{p0}	particle number in a section
Nu	Nusselt number
NuI	Nusselt number increment
p, P	non-dimensional and dimensional pressure, Pa
PC	performance coefficient
Pe	Peclet number
Pr	Prandtl number
q	heat flux, $W.m^{-2}$
r	Distance from the center, m
Re	Reynolds number
Re_p	Particle Reynolds number
Sb	Subcooling number
Ste	Stephane Number
t	time, s
T	non-dimensional temperature
U, V	velocity component in x,y directions, $m.s^{-1}$
u, v	non-dimensional velocity component in x,y directions
X, Y	x,y coordinate, m
x, y	non-dimensional x,y coordinate
<i>Greek Symbols</i>	
α	Thermal diffusion coefficient, $m^2.s^{-1}$
δ	domain thickness, m
δV	The volume of the Eulerian cell, m^3
θ	temperature, K
μ	viscosity, Pa.sec
ρ	density, $kg.m^{-3}$
ϕ	Particle volume concentration
φ	the volume of the shell to the volume of the particle ratio
Δt^*	Non-dimensional time step
<i>Superscripts</i>	
*	non-dimensional parameters
<i>Subscripts</i>	
0	Pure fluid
1	Inner diameter
2	Outer diameter
b	slurry bulk value, buoyancy
c	cold boundary
C	Particle shell
D	Drag force
f	Fluid
g	Gravity
h	hot boundary
i	Internal particle diameter, m
l	Liquid
m, M	working fluid (mixed fluid and particles)
p	Particle
ps	Particle surface
PCM	Phase change material
s	Solid
x	Local Nusselt number

1. Introduction

Slurry fluids which are made of base fluid containing the PCM particles are used to increase the heat transfer coefficient. In this mixed fluids, microencapsulated PCMs absorb the heat of their surrounded fluid and while the temperature of the particle does not increase much, they reduce the temperature of their surrounding fluid.

Nowadays, with the advancement of industry and the growth of technology, the size of equipment, such as some electronic components, has become smaller. Some of these components, such as CPUs, generate a lot of heat. The small surface of these tiny devices produces a lot of heat flux. One of the ways to increase the heat transfer rate in these devices is to use the microencapsulated PCM as a slurry in these components. PCMs usually have a low thermal conductivity and high latent heat value. The first characteristic is their weaknesses and the second one is their strengths. Cooling these tiny electronic devices, can be improved, due to the high latent heat of these materials. Another application of these slurry flows is using them in the chilled ceiling [1, 2].

Many researchers have studied cooling by the slurry flows containing PCM materials. Safdari et al. [3] have examined the use of a PCM layer in the various forms as a passive and air as an active coolant in a battery. Batteries which contain PCMs, have been studied in three different shapes with circular, square and hexagonal cross-sections with the same area. Thermal performance for both circular and hexagonal shapes is almost the same. Heat storage systems have been widely studied as latent heat to cover energy supply and demand differences by Yan et al. [4]. They examined the storage of latent heat inside a pipe by PCM materials numerically and experimentally. In this work, PCM material has been used once in the internal part and once in the external part. Their results show that the presence of PCM in the inner part of the pipe performs better. Natural convection in a cavity containing PCM nanoparticles has been studied, using homogeneous single-phase model numerically by Ghalambaz et al. [5]. In this case, the particles near the hot wall reduce the temperature of the surrounding fluid by receiving heat while melting, and the particles near the cold wall, increase the temperature of the surrounding fluid by releasing heat while freezing. They will affect the temperature of the surrounding fluid. They reported a 10 percent increase in heat transfer coefficient.

There are a number of ways to solve the heat transfer problem of encapsulated PCM materials, including a homogeneous one phase method, which assumes that the slurry fluid is a homogeneous solution, and for calculation of the properties, including density, viscosity, heat capacity and thermal conductivity, researchers use the two-phase relations in this method. The results of this method are far from the experimental results [6], which are obtained for the metal nanoparticles. It is the major weakness of this method. Another method that is more complicated is the Eulerian-Lagrangian two-phase model, which is used in this paper. In this method, the velocity, location and temperature of the particles are obtained by tracking the particles. Rostami et al. [6] investigated convective heat transfer by nanoparticles in a wavy microchannel by Eulerian-Lagrangian method. Due to the large number of particles (up to 32 million particles), their calculations were performed using a parallel processing technique by 256 CPUs of a supercomputer with 1400 cores. In this method, due to the non-dependence of the particle results on each other, the total number of particles is divided into the number of computer cores, and each core solve the governing equations of a certain particles.

Kalteh et al. [7] investigated the nanofluid flow in a rectangular microchannel using a two-phase model. They studied it for water- Al_2O_3 nanofluid in different volume fraction experimentally and solved the governing equations using a control volume method for both phases numerically. Their results show that there is not much difference between the velocity and temperature of the two phases, but the two-phase model reports more heat transfer coefficient than the single-phase model, and the results of the two-phase model are closer to the experimental results.

Mirzaei et al. [8] also used the Eulerian-Lagrangian method to study the heat transfer in the entrance length of a micro-channel with constant wall temperature boundary condition. Their results also confirm that the results of this method are closer to the experimental results in compare with the results of the one phase model.

The results of [6-8] show that in compare with the homogeneous method the obtained Nusselt number from the two-phase model (Eulerian-Lagrangian) are closer to the experimental results. Then, in this paper, the problem has been investigated via Eulerian-Lagrangian two-phase model. Also, due to the high Biot number of PCM particles, the lumped temperature assumption is not valid for this tiny particles and, in this study the transient one dimensional conduction equation has been solved for each particle. Then, one of the main purposes of this work is presenting the numerical details of solving the temperature equation in the PCM particles.

2. Governing Equations and Boundary Conditions

Fig. 1, shows the geometry of the annular tube. The inner and outer diameters of the tube are 1mm and 3 mm respectively. It contains the microencapsulated PCMs with 10 micrometer diameter. Based on the Reynolds number, the length of the pipe is chosen so that the flow is developed hydrodynamically for higher Reynolds number ($\text{Re}=500$) and the last 10% of the pipe length is insulated. Assuming the homogenous distribution of the particles in angular direction, the solution area is also selected as a slit of the tube.

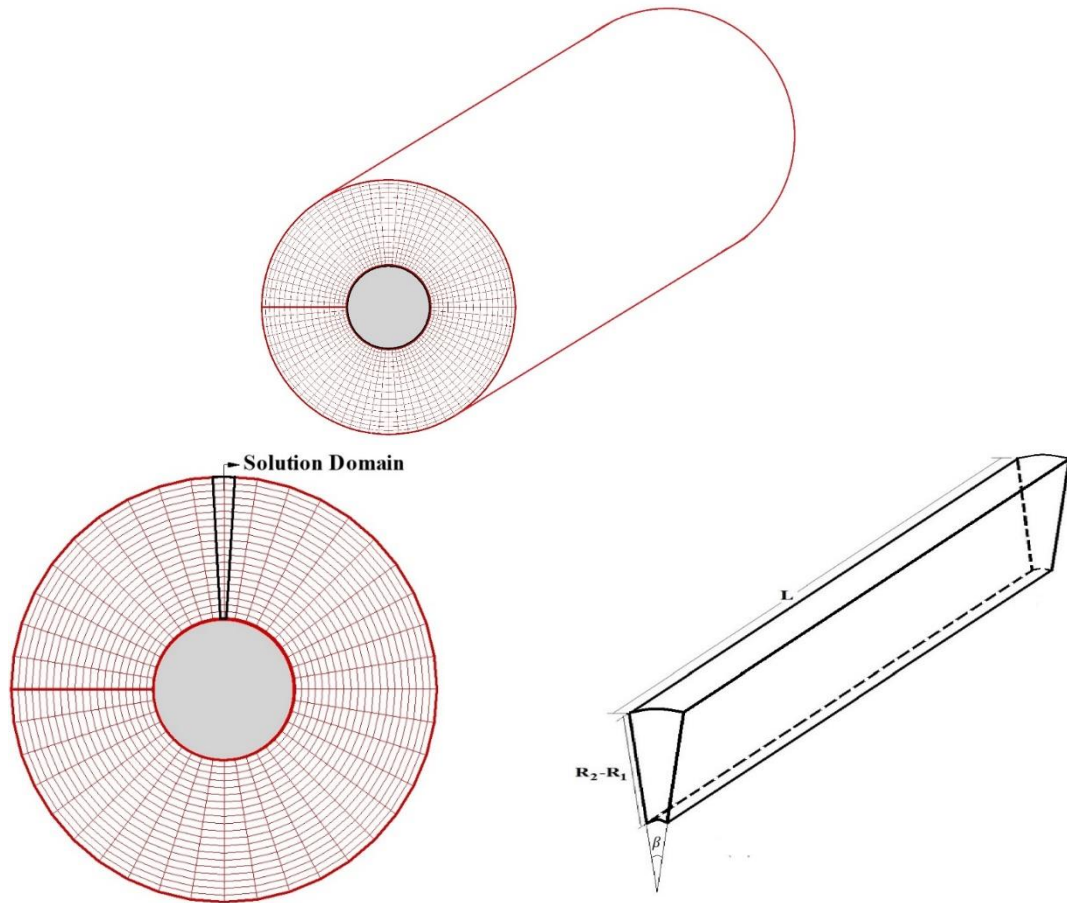


Fig. 1: The geometry and the solution domain of the mini-pipe containing water and encapsulated PCM particles.

Solution domain is shown Fig. 1. Due to the location of the particles away from the walls and to ensure the complete placement of each particle inside the solution area, the lower arc length of the solution domain is equal to the particle diameter. i.e. $0.5D_1\beta = D_p$. The β angle is obtained as follow,

$$\beta = \frac{2D_p}{D_1}, \tag{1}$$

By defining the volumetric concentration (total volume of particles to the volume of the solution domain) as,

$$\phi = \frac{N_p \frac{\pi}{6} D_p^3}{\frac{\beta}{8} (D_2^2 - D_1^2) L}. \tag{2}$$

Then, the total number of particles is obtained using Eqs. (1, 2),

$$N_p = \frac{3(D_2^2 - D_1^2) L \phi}{2\pi D_1 D_p^2}. \tag{3}$$

One of the methods of numerical solution of heat transfer in a fluid containing encapsulated PCM is the one phase homogeneous method. However, due to the non-homogeneous distribution of particles, the results of this method do not have the accuracy of the two-phase method [6, 8]. One of the two phase methods is Eulerian-Lagrangian method. In Lagrangian's view, particles are tracked and the effect of the fluid velocity and temperature on the particles position, velocity and temperature are investigated. In turn, the effect of particles, which appear as source terms in Eulerian equations, is also considered.

In this paper, the two-phase Eulerian-Lagrangian method is used to solve the problem. In this method, the effect of both phases on each other is considered. In the other words, the effect of phases on each other is two-way.

By the following dimensionless parameters and using hydraulic diameter as $D_h = D_2 - D_1$,

$$\begin{aligned} \phi_f &= 1 - \phi, x = \frac{X}{D_h}, r^* = \frac{r}{D_h}, d_p = \frac{D_p}{D_h}, t^* = \frac{U_b t}{D_h}, u_i = \frac{U_i}{U_b}, p = \frac{P}{\rho_f U_b^2}, T = \frac{\theta - \theta_c}{\theta_h - \theta_c} \\ Pr &= \frac{\mu_f C p_f}{k_f}, Re = \frac{\rho_f U_b D_h}{\mu_f}, Pe = Re \cdot Pr, Ste = \frac{C p_p (\theta_l - \theta_s)}{L_{sl}} \end{aligned} \quad (4)$$

the fluid phase governing equations in the polar coordinate are as follows [9], continuity:

$$\frac{\partial \phi_f u}{\partial x} + \frac{1}{r^*} \frac{\partial \phi_f r^* v}{\partial r^*} = 0, \quad (5)$$

momentum:

$$\frac{\partial \phi_f u \psi}{\partial x} + \frac{1}{r^*} \frac{\partial \phi_f r^* v \psi}{\partial r^*} = S_{P\psi} + \left[\frac{\partial}{\partial x} \left(\frac{\phi_f}{Re} \frac{\partial \psi}{\partial x} \right) + \frac{1}{r^*} \frac{\partial}{\partial r^*} \left(\frac{\phi_f}{Re} \frac{\partial r^* \psi}{\partial r^*} \right) \right] - \frac{\rho_p \pi d_p^3}{\rho_f 6 \delta V^*} \sum_{np} \frac{d\psi_p}{dt^*}, \quad (6)$$

where ψ denotes u and v. The last sentence in this equation, is a generated source term by the particles [9] and n_p and δV^* are the number of particles in an Eulerian cell and the volume of the cell, respectively. Furthermore,

$$S_{Pu} = -\phi_f \frac{\partial p}{\partial x}, \quad (7)$$

$$S_{Pv} = -\phi_f \frac{\partial p}{\partial r^*}, \quad (8)$$

and the volume of the Eulerian cells can be obtained by,

$$\delta V^* = r^* \beta \Delta x \Delta r^*. \quad (9)$$

Using Eq. (1),

$$\delta V^* = 2r^* \frac{d_p}{d_1} \Delta x \Delta r^*, \quad (10)$$

then, using Eq. (9) and multiplying the Eq. (6) by r^* the Eq. (6) changes to,

$$r^* \frac{\partial \phi_f u \psi}{\partial x} + \frac{\partial \phi_f r^* v \psi}{\partial r^*} = r^* S_{P\psi} + \left[r^* \frac{\partial}{\partial x} \left(\frac{\phi_f}{Re} \frac{\partial \psi}{\partial x} \right) + \frac{\partial}{\partial r^*} \left(\frac{\phi_f}{Re} \frac{\partial r^* \psi}{\partial r^*} \right) \right] - \frac{\rho_p \pi d_p^2 d_1}{\rho_f 12 \Delta x \Delta r^*} \sum_{np} \frac{d\psi_p}{dt^*}. \quad (11)$$

Energy equation [9] is,

$$r^* \frac{\partial \phi_f u T}{\partial x} + \frac{\partial \phi_f r^* v T}{\partial r^*} = \left[r^* \frac{\partial}{\partial x} \left(\frac{\phi_f}{Pe} \frac{\partial T}{\partial x} \right) + \frac{\partial}{\partial r^*} \left(\frac{\phi_f}{Pe} \frac{\partial r^* T}{\partial r^*} \right) \right] - \frac{\rho_p}{\rho_f C p_f} \frac{1}{12 \Delta x \Delta r^*} \frac{\pi d_p^2 d_1}{np} \sum \frac{dh_p}{dt^*}, \quad (12)$$

the enthalpy of the particles is calculated as follows [10],

$$h_p = h_s + \lambda L_{sl}, \lambda = \frac{T - T_s}{T_l - T_s}, T_s < T < T_l \text{ (while melting)} \quad (13)$$

where T_s is the starting temperature of the PCM melting and T_l is the final temperature of the melting process. Using Ste number definition in Eq. (3), the energy equation will be as follows.

$$\frac{\partial \phi_f u T}{\partial x} + \frac{1}{r^*} \frac{\partial \phi_f r^* v T}{\partial r^*} = \left[\frac{\partial}{\partial x} \left(\frac{\phi_f}{Pe} \frac{\partial T}{\partial x} \right) + \frac{1}{r^*} \frac{\partial}{\partial r^*} \left(\frac{\phi_f}{Pe} \frac{\partial r^* T}{\partial r^*} \right) \right] - \frac{1}{Ste} \frac{\rho_p C p_p}{\rho_f C p_f} \frac{\pi d_p^2 d_1}{12 \Delta x \Delta r^*} \sum_{np} \frac{dT_p}{dt^*}. \quad (14)$$

The particle phase governing equation in Lagrangian view:

The detailed of these governing equations are presented by Wen et al. [11].

Velocity

The thickness of the Fe_3O_4 as the cover of the particles has been chosen such a way to density of the particle be equal to density of the based fluid. This calculation has been presented in [12]. Then, the buoyancy force of the particles is equal to the weight of the particles and it doesn't appear in the Eqs. (16, 17).

By defining CD number as [11],

$$CD = \frac{18}{Re} \frac{\rho_f}{d_p^2 \rho_p} (1 + 0.15 Re_p^{0.687}) \quad (15)$$

the velocity components of the particle will be achieved by,

$$\frac{du_p}{dt^*} = CD(u_f - u_p) \quad (16)$$

$$\frac{dv_p}{dt^*} = CD(v_f - v_p) \quad (17)$$

and the particle position is obtained by the following relations,

$$dx_p = u_p dt^*, \quad (18)$$

$$dy_p = v_p dt^*. \quad (19)$$

Energy

As mentioned in [12] the Biot number for PCM is bigger than 0.1. Then the particle temperature is not uniform (lump) and the energy equation for PCM is,

$$\frac{\partial T_p}{\partial t^*} = \frac{\alpha_p}{\alpha_f} \frac{Ste}{Pe} \frac{1}{r^{*2}} \frac{\partial}{\partial r^*} \left(r^{*2} \frac{\partial T_p}{\partial r^*} \right) \quad (20)$$

where α is thermal diffusion coefficient.

Boundary conditions

At the inlet, velocity and temperature are uniform. Then,

$$u(0, r^*) = 1, v(0, r^*) = 0, T(0, r^*) = 0 \quad (21)$$

Before the outlet boundary, 10% of the wall is assumed to be insulated. Then, the following boundary condition is applied for the velocity and temperature,

$$\left. \frac{\partial u}{\partial x} \right|_{(L^*, r^*)} = 0, \left. \frac{\partial v}{\partial x} \right|_{(L^*, r^*)} = 0, \left. \frac{\partial T}{\partial x} \right|_{(L^*, r^*)} = 0. \quad (22)$$

On the inner pipe wall,

$$u(x, 0.25) = 0, v(x, 0.25) = 0, \begin{cases} T(x, 0.25) = 1, 0 < x < 0.9L^* \\ \left. \frac{\partial T}{\partial r^*} \right|_{(x, 0.25)} = 0, 0.9L^* < x < L^* \end{cases} \quad (23)$$

and on the outer pipe wall,

$$u(x, 0.75) = 0, v(x, 0.75) = 0, \begin{cases} T(x, 0.75) = 1, 0 < x < 0.9L^* \\ \left. \frac{\partial T}{\partial r^*} \right|_{(x, 0.75)} = 0, 0.9L^* < x < L^* \end{cases} \quad (24)$$

3. Numerical Procedure

The problem has been modeled in the two phase model by Eulerian-Lagrangian method. The fluid phase governing equations are solved by a control volume (SIMPLE) method [13]. To avoid the checkerboard pressure, the Rhie and Chow [14] interpolation for the velocity in the pressure correction equation was used. Also, for the convective terms calculation, the Hybrid difference scheme [15] was used. To solve the governing equations for particle velocities, the 4th order of Runge-Kutta method has been used. The two-way coupling between the particles and the fluid is assumed, and the exchange of results between the fluid and particle phases continues until the mean Nusselt number is converged to a constant value. In this method, to solve the velocity and temperature of the particles, the velocity and temperature of its surrounding fluid is needed. For this purpose, first the location of the particle and its Eulerian cell is determined. Then the velocity and temperature of the fluid around the particle are averaged from the four corners of that Eulerian

cell. Now, with the defined velocity components, the location of the particle at each time step is determined. More detailed of the numerical procedure has been presented in the previous work [12].

Details of solving the particle temperature

Using the fully implicit method to discretize the Eq. (20), leads to,

$$\frac{(T_i^n - T_i^{n-1})}{\Delta t^*} = \frac{\alpha_p Ste}{\alpha_f Pe} \frac{1}{r_i^{*2}} \frac{1}{\Delta r^*} \left[\left(\frac{r_{i+1}^* + r_i^*}{2} \right)^2 \frac{T_{i+1}^n - T_i^n}{\Delta r^*} - \left(\frac{r_i^* + r_{i-1}^*}{2} \right)^2 \frac{T_i^n - T_{i-1}^n}{\Delta r^*} \right], \quad (25)$$

where up scripts “n” refers to the present time and “n-1” refers to the last step time.

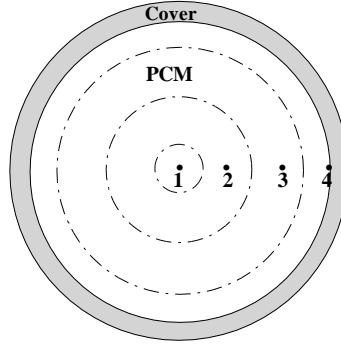


Fig. 2. One dimensional grid in a particle.

As shown in Fig. 2, four nodes are used in the particles. Then $\Delta r^* = \frac{d_i}{6}$, where d_i is the internal diameter of a particle.

By defining λ as,

$$\lambda = 0.25 \frac{\alpha_p Ste \Delta t^*}{\alpha_f Pe \Delta r^{*2}} = 9 \frac{\alpha_p Ste \Delta t^*}{\alpha_f Pe d_i^2}, \quad (26)$$

It can be rearranged as,

$$-\lambda \left(\frac{r_{i-1}^*}{r_i^*} + 1 \right)^2 T_{i-1}^n + \left[1 + \lambda \left(\frac{r_{i+1}^*}{r_i^*} + 1 \right)^2 + \lambda \left(\frac{r_{i-1}^*}{r_i^*} + 1 \right)^2 \right] T_i^n - \lambda \left(\frac{r_{i+1}^*}{r_i^*} + 1 \right)^2 T_{i+1}^n = T_i^{n-1}. \quad (27)$$

and for nodes 2 and 3,

$$i = 2: -\lambda \left(\frac{r_1^*}{r_2^*} + 1 \right)^2 T_1^n + \left[1 + \lambda \left(\frac{r_3^*}{r_2^*} + 1 \right)^2 + \lambda \left(\frac{r_1^*}{r_2^*} + 1 \right)^2 \right] T_2^n - \lambda \left(\frac{r_3^*}{r_2^*} + 1 \right)^2 T_3^n = T_2^{n-1}, \quad (28)$$

$$i = 3: -\lambda \left(\frac{r_2^*}{r_3^*} + 1 \right)^2 T_2^n + \left[1 + \lambda \left(\frac{r_4^*}{r_3^*} + 1 \right)^2 + \lambda \left(\frac{r_2^*}{r_3^*} + 1 \right)^2 \right] T_3^n - \lambda \left(\frac{r_4^*}{r_3^*} + 1 \right)^2 T_4^n = T_3^{n-1}. \quad (29)$$

Due to the uniform grid in the particle $r_i^* = (i - 1)\Delta r^*$, then,

$$i = 2: -\lambda(1)^2 T_1^n + [1 + \lambda(3)^2 + \lambda(1)^2] T_2^n - \lambda(3)^2 T_3^n = T_2^{n-1}, \quad (30)$$

$$i = 3: -\lambda(1.5)^2 T_2^n + [1 + \lambda(2.5)^2 + \lambda(1.5)^2] T_3^n - \lambda(2.5)^2 T_4^n = T_3^{n-1}. \quad (31)$$

Finally,

$$i = 2: -\lambda T_1^n + (1 + 10\lambda) T_2^n - 9\lambda T_3^n = T_2^{n-1}, \quad (32)$$

$$i = 3: -2.25\lambda T_2^n + (1 + 8.5\lambda) T_3^n - 6.25\lambda T_4^n = T_3^{n-1}. \quad (33)$$

Due to symmetry,

$$T_1^n = T_2^n. \tag{34}$$

Because the Biot number for shell (thin metal) is less than 0.1, the temperature of the shell of the particles, assumed to be lumped. Then the energy conservation in the cover, $\dot{E}_{store} = \dot{E}_{in} - \dot{E}_{out}$ leads to,

$$m_c C p_c \frac{\partial \theta}{\partial t} = -k_c \pi D_i^2 \left. \frac{\partial \theta}{\partial r} \right|_{r=0.5D_i} - h \pi D_p^2 (\theta_f - \theta). \tag{35}$$

First term of the right hand side is \dot{E}_{in} , which inlet the cover by conduction mechanism from the PCM and the second term is \dot{E}_{out} which leaves the cover and inlet the surrounding fluid by convection mechanism. Also, “h” is obtained from [16] as bellow,

$$Nu = \frac{h D_p}{k_f} = 2 + 0.6 Re_p^{0.5} Pr^{\frac{1}{3}}. \tag{36}$$

Then, in the dimensionless form,

$$\rho_c (d_p^3 - d_i^3) C p_c U_b \frac{\partial T}{\partial t^*} = -6 k_c d_i^2 \left. \frac{\partial T}{H \partial r^*} \right|_{r^*=0.5d_i} - 6 h d_p^2 (T_f - T). \tag{37}$$

Discretizing this equation leads to,

$$\rho_c (d_p^3 - d_i^3) C p_c U_b \frac{T_4^n - T_4^{n-1}}{\Delta t^*} = -6 k_c d_i^2 \left. \frac{T_4^n - T_3^n}{H \Delta r^*} \right|_{r^*=0.5d_i} - 6 h d_p^2 (T_f - T_4^n). \tag{38}$$

By defining,

$$A = \frac{\rho_f C p_f}{\rho_c C p_c} \frac{6 \Delta t^*}{(d_p^3 - d_i^3) Pe} \tag{39}$$

$$B = 6 A d_i \frac{k_c}{k_f} \tag{40}$$

we have

$$T_4^n = \frac{T_4^{n-1} + B T_3^n + A Nu d_p T_f}{1 + B + A Nu d_p}, \tag{41}$$

then the set of the equations for a particle is as follows,

$$T_1^n = T_2^n \tag{42}$$

$$-\lambda T_1^n + (1 + 10\lambda) T_2^n - 9\lambda T_3^n = T_2^{n-1} \tag{43}$$

$$-2.25\lambda T_2^n + (1 + 8.5\lambda) T_3^n - 6.25\lambda T_4^n = T_3^{n-1} \tag{44}$$

$$-B T_3^n + (1 + B + A Nu d_p) T_4^n = T_4^{n-1} + A Nu d_p T_f \tag{45}$$

Substituting Eq. (42) in Eq. (43) concise it to,

$$(1 + 9\lambda) T_2^n - 9\lambda T_3^n = T_2^{n-1}. \tag{46}$$

By replace T_4^n from Eq. (41) in (44), we have,

$$-2.25\lambda T_2^n + (1 + 8.5\lambda) T_3^n - 6.25\lambda \frac{T_4^{n-1} + B T_3^n + A Nu d_p T_f}{1 + B + A Nu d_p} = T_3^{n-1}, \tag{47}$$

or

$$-2.25\lambda(1 + B + A.Nu.d_p)T_2^n + [(1 + 8.5\lambda)(1 + B + A.Nu.d_p) - 6.25\lambda B]T_3^n = \quad (48)$$

$$T_3^{n-1} + 6.25\lambda(T_4^{n-1} + A.Nu.d_p.T_f).$$

Now, the unknown temperature have been reduced to T_2^n and T_3^n in Eqs. (46, 48). By introduce the following variables,

$$C = 1 + 9\lambda, D = -9\lambda E = T_2^{n-1} \quad (49)$$

$$F = -2.25\lambda(1 + B + A.Nu.d_p) \quad (50)$$

$$G = [(1 + 8.5\lambda)(1 + B + A.Nu.d_p) - 6.25\lambda B] \quad (51)$$

$$H = (1 + B + A.Nu.d_p)T_3^{n-1} + 6.25\lambda(T_4^{n-1} + A.Nu.d_p.T_f), \quad (52)$$

these Eqs. (46, 48) can be showed by,

$$\begin{bmatrix} C & D \\ F & G \end{bmatrix} \begin{bmatrix} T_2^n \\ T_3^n \end{bmatrix} = \begin{bmatrix} E \\ H \end{bmatrix}. \quad (53)$$

By solving this set,

$$\begin{bmatrix} T_2^n \\ T_3^n \end{bmatrix} = \frac{1}{CG-DF} \begin{bmatrix} G & -D \\ -F & C \end{bmatrix} \begin{bmatrix} E \\ H \end{bmatrix}, \quad (54)$$

and, placement them in Eqs. (42, 45), all the unknown temperatures in the particle will be obtained as follows,

$$T_2^n = \frac{GE - DH}{CG - DF}, \quad (55)$$

$$T_1^n = T_2^n, \quad (56)$$

$$T_3^n = \frac{-FE + CH}{CG - DF}, \quad (57)$$

$$T_4^n = \frac{T_4^{n-1} + BT_3^n + A.Nu.d_p.T_f}{1 + B + A.Nu.d_p}. \quad (58)$$

Then, the temperatures of all nodes of a particle in the present time can be calculated using their temperatures from the last step time and the temperature of the surrounding fluid.

The local Nusselt number is calculated as follow,

$$Nu_x = \frac{hD_h}{k_b} = \frac{q''D_h}{k_b(\theta_w - \theta_b)} = \frac{-\left(k_m \frac{\partial \theta}{\partial r}\Big|_{r=R_1} + k_m \frac{\partial \theta}{\partial r}\Big|_{r=R_2}\right)D_h}{k_M(\theta_w - \theta_b)}$$

$$= -\frac{1}{(1 - T_b)} \frac{k_m}{k_M} \left(\frac{\partial T}{\partial r^*}\Big|_{r^*=0.25} + \frac{\partial T}{\partial r^*}\Big|_{r^*=0.75} \right), \quad (59)$$

where k_m is the local thermal conductivity in a cell and k_M is the average thermal conductivity [17] and is obtained by,

$$k_M = (1 - \phi)k_f + \phi k_p, \quad (60)$$

where ϕ is the average volume concentration. This relation is also used for calculating k_m using local ϕ . The mean Nusselt number is calculated by,

$$Nu = \frac{1}{0.9L} \int_{x=0}^{x=0.9L} Nu_x dx = \frac{1}{0.9L^*} \int_{x=0}^{x=0.9L^*} Nu_x dx. \quad (61)$$

In the slurry fluid, the bulk temperature is calculated as follow,

$$T_b = \frac{6(\rho Cp)_f \int \phi_f u_f T_f dV^* + (\rho Cp)_p \pi d_p^3 \sum_{np0} u_p T_p}{(\rho Cp)_M (6\phi_f V_0^* + n_{p0} \pi d_p^3)}, \quad (62)$$

where n_{p0} is the number of the particles in each section and V_0 is obtained by cells volume summation in each section, and, $(\rho Cp)_M$ is the heat capacity of the working fluid and is calculated by the following relation,

$$(\rho Cp)_M = (1 - \phi)(\rho Cp)_f + \phi(\rho Cp)_p. \tag{63}$$

In Eq. (62), T_p is particle mean temperature and is obtained by the following relation,

$$\begin{aligned} (\rho Cp)_p \frac{\pi}{6} D_p^3 T_p = & (\rho Cp)_{PCM} \frac{\pi}{6} \Delta r^3 T_p(1) + (\rho Cp)_{PCM} \frac{\pi}{6} [(3\Delta r)^3 - \Delta r^3] T_p(2) + \\ (\rho Cp)_{PCM} \frac{\pi}{6} [(5\Delta r)^3 - (3\Delta r)^3] T_p(3) + & (\rho Cp)_{PCM} \frac{\pi}{6} [(6\Delta r)^3 - (5\Delta r)^3] T_p(4) + \\ (\rho Cp)_c \frac{\pi}{6} (d_p^3 - d_i^3) T_p(4). & \end{aligned} \tag{64}$$

By simplifying and placement $T_p(1) = T_p(2)$, finally,

$$\begin{aligned} 216(\rho Cp)_p \frac{d_p^3}{d_i^3} T_p = & 27(\rho Cp)_{PCM} T_p(2) + 98(\rho Cp)_{PCM} T_p(3) + 91(\rho Cp)_{PCM} T_p(4) + \\ 216(\rho Cp)_c \left(\frac{d_p^3}{d_i^3} - 1 \right) T_p(4) & \end{aligned} \tag{65}$$

4. Results and Discussions

Properties of water and paraffin wax have been presented in the previous work [12]. The validation of the results for ReCf and Nusselt numbers is shown in a tube with a constant temperature boundary condition without the presence of particles in Fig. 3, for Re=120 and Pr=1. It is observed that the ReCf starts from a large value at the inlet of the pipe and tends to a constant value of 16 [18-20] in the developed region. The Nusselt number also starts with a certain value and tends to 3.66 [18-20] in the developed region. Also, the velocity profile in the developed region, has been compared with analytical solution (Eq. 66) and the results are in a good agreement.

$$u(r) = \frac{2}{\frac{R_2^2 + R_1^2}{R_2^2 - R_1^2} - \frac{1}{\ln\left(\frac{R_2}{R_1}\right)}} \left[\frac{\ln\left(\frac{r}{R_1}\right)}{\ln\left(\frac{R_2}{R_1}\right)} - \frac{r^2 - R_1^2}{R_2^2 - R_1^2} \right] \tag{66}$$

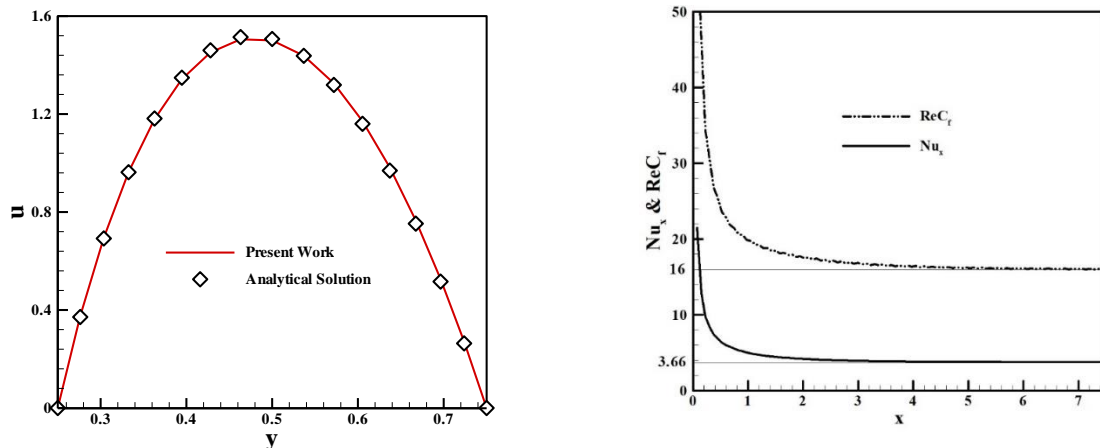


Fig. 3. Code validity for Re=120 and Pr=1.

According to the author’s knowledge, there were no experimental results for microencapsulate PCM slurry flow heat transfer. However, the results of the Eulerian-Lagrangian method in the previous work of the author [6] have been compared with experimental work [21] for metal nanoparticles and the results were adapted well.

The grid independency has also been investigated and the code has been run for different grid points. The difference in the obtained Nusselt number for 100×20 and 120×24 points was so close together, and, the different in the Nusselt number is less than 2%. Then, the 100×20 points used for calculations.

Table 1: Grid independency

Nx-Ny	Nu	Error%
60×12	11.54	8.99
80×16	12.10	4.57
100×20	12.44	1.85
120×24	12.68	-

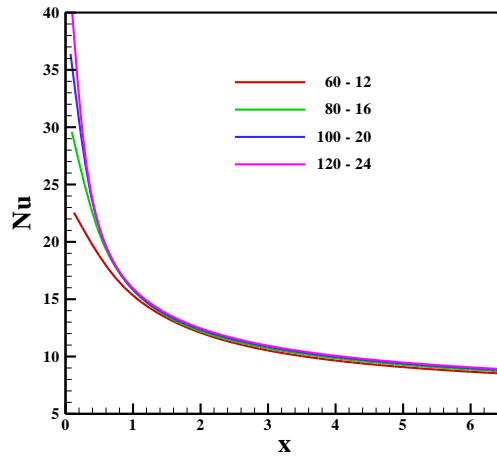


Fig. 4. Grid independency study for pure water at $Re=500$.

Fig. 5, shows the particle distribution. Fig. 5(a) shows the particles location at the final time. It is observed that the particles are distributed far from the walls. Fig. 5(b) shows the volume fraction of particles in the middle section of the pipe. It is clear that, the volume fraction of particles in a layer slightly far from the wall (after the particle-free space) is higher than the average volume fraction. In other words, particles spaced from the wall accumulate in this space. This has also been confirmed by [8]. Furthermore, the local volume fraction near the inner wall is more than that near the outer wall. It has happened due to the vertical velocity component, which sends the particles toward the inner wall.

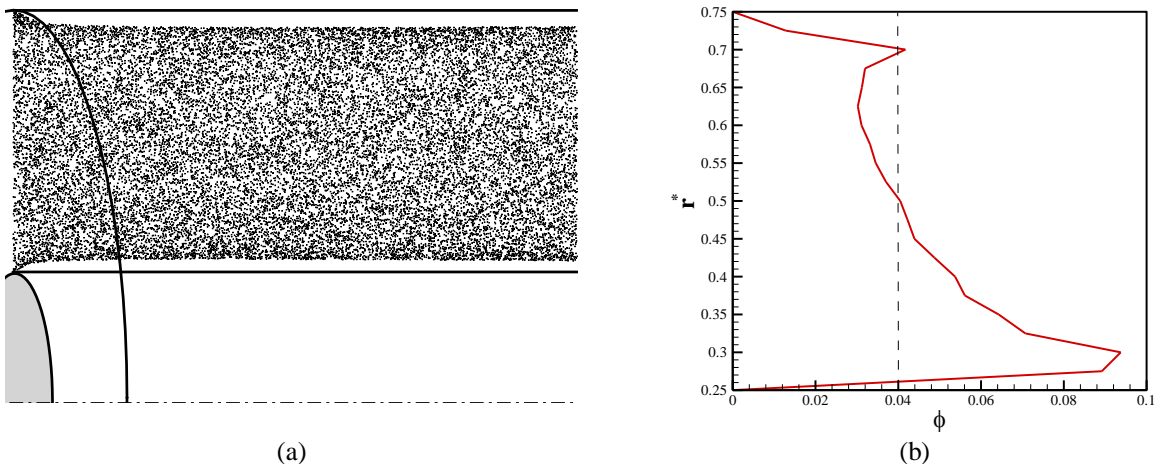


Fig. 5. (a) particle distribution (b) local particle concentration profile at $Re=500$, $\phi = 0.04$.

This figure shows that the particle distribution in the solution area is not uniform and the results of one phase homogeneous method is far from the experimental results as shown in [6,8]. This is due to the vertical component of the fluid velocity in the entrance length region, which causes drag force to carry particles and place them at a distance from the wall.

The path of the particles is also shown in Fig. 6. The path of the particles and their movement away from the wall is confirmed. It can be seen, that, the path of the particles is closer to the inner wall in compare with the outer wall. The non-dimensional distance of the particles from the inner wall is 0.034 and is 0.051 for the outer wall, i.e. the distance of particles from outer wall is 1.5 times more than the distance of the particles from the inner wall.

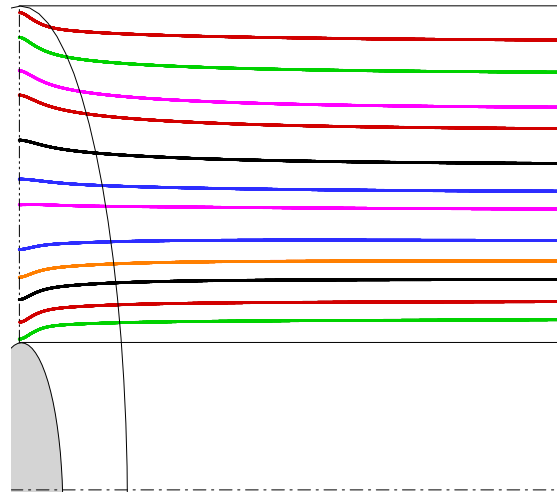


Fig. 6. The trace of the random selected particles.

The fluid bulk temperature is shown in Fig. 7. It is observed that, due to the presence of the particles as distributed heat sinks, by volume fraction increasing, the fluid bulk temperature decreases. This cools the base fluid and able it to absorb more heat flux from the wall.

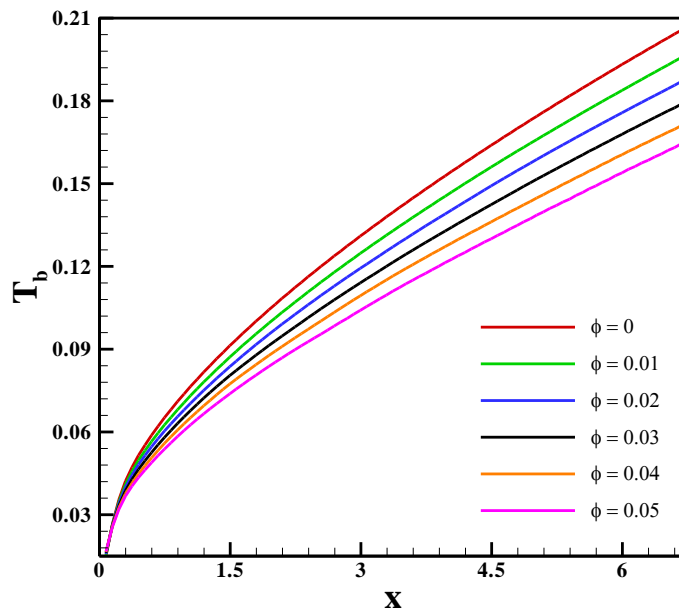


Fig. 7. Working fluid bulk temperature for Re=350 at different volume concentration.

The presence of PCM particles reduces the thickness of the thermal boundary layer and thus reduces the fluid thermal resistance as shown in Fig. 8. This will increase the temperature gradient near the body and thus increase the absorbed heat flux from walls. The received heat flux from the wall is also shown in Fig. 9. It is observed that at each section the heat flux is greater for the higher volume fraction.

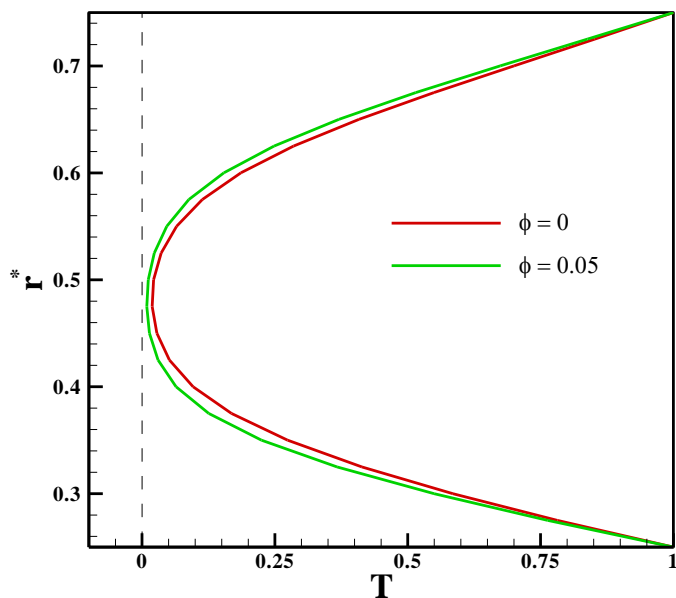


Fig. 8. the temperature profile in the middle of the pipe length for $Re=200$.

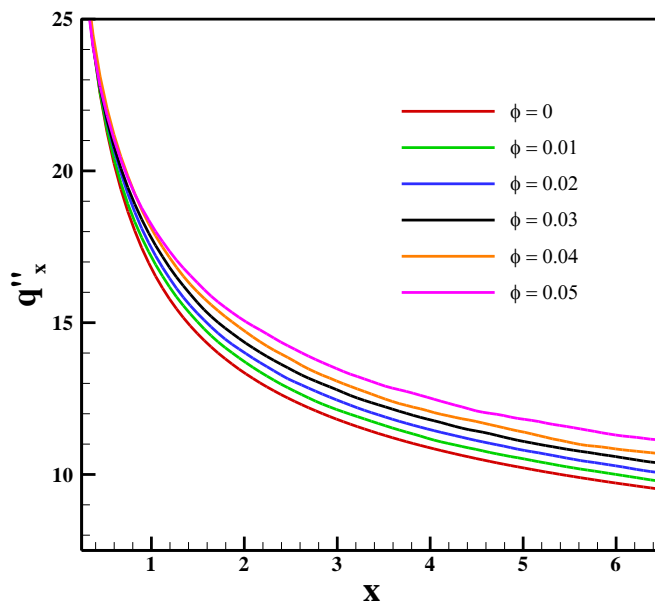


Fig. 9. Wall heat flux for $Re=500$ at different volume concentration.

The local Nusselt number for $Re=500$ is calculated based on Eq. (59), and shown in Fig. 10. It is clear that, the local Nusselt number increases with increasing the volume fraction at each section. The mean Nusselt number is also plotted by integrating the local Nusselt number according to Eq. (61) in Fig. 11, for different Reynolds numbers at different concentrations.

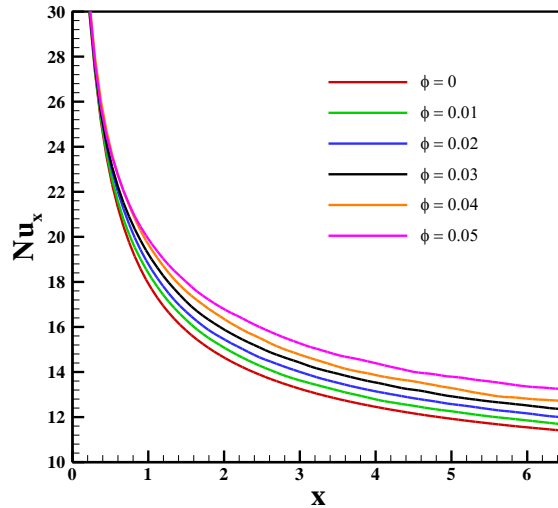


Fig. 10. Local Nusselt number for Re=500 at different volume concentration.

It is observed that the mean Nusselt number increases linearly with the volume fraction. This increase in the Nusselt number with the volume fraction is expressed by the following equation with maximum error less than 1%.

$$Nu = Nu_0 + 2.3937Re^{0.441} \phi, \quad 0 \leq \phi \leq 0.05, \quad 200 \leq Re \leq 500, \tag{67}$$

where subscript “0” refers to the Nusselt number for pure fluid.

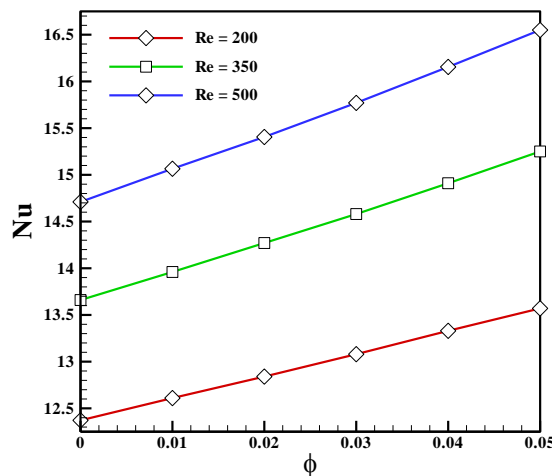


Fig. 11. Mean Nusselt number for different Reynolds number vs. volume concentration.

In convective heat transfer problems, both the heat transfer coefficient and the rate of pressure drop are important. Presence of microencapsulated PCMs increases the pressure drop slightly, it is due to the equality of the density of the base and slurry fluid, but, it increases the Nusselt number more sensitive.

The friction factor is obtained by the following equation,

$$f = 2 \frac{\Delta p}{\Delta x}. \tag{68}$$

The increase of friction factor is presented in Fig. 12 for different Reynolds numbers. It is clear that, as the particle concentration increases, the friction factor increases linearly. The maximum increase in the friction factor is just 5% and is occurred for Re=500. For other states, the increasing in friction factor is less than 5%.

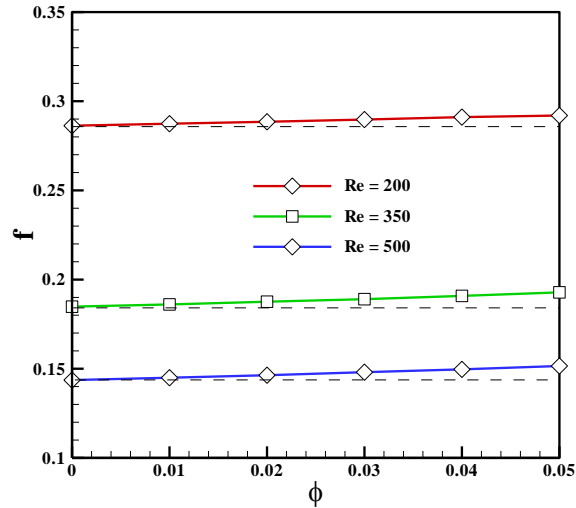


Fig. 12. Friction factor for different Reynolds number vs. particle concentration.

Another criterion to judge about increasing in the heat transfer rate and in the friction factor is present them in the following formulas,

$$NuI = \frac{Nu - Nu_0}{Nu_0}, \quad (69)$$

$$fI = \frac{f - f_0}{f_0}. \quad (70)$$

Both of these new parameters are shown in Fig. 13. It is clear that the maximum increase in the Nusselt number and the friction factor is occurred for Re=500 and $\phi = 0.05$. It can be concluded that the increase in the heat transfer rate is more than the increase in the friction factor and it is a good news. Because the researchers in the convective heat transfer are searching for situations having high heat transfer coefficient and low pressure drop penalty.

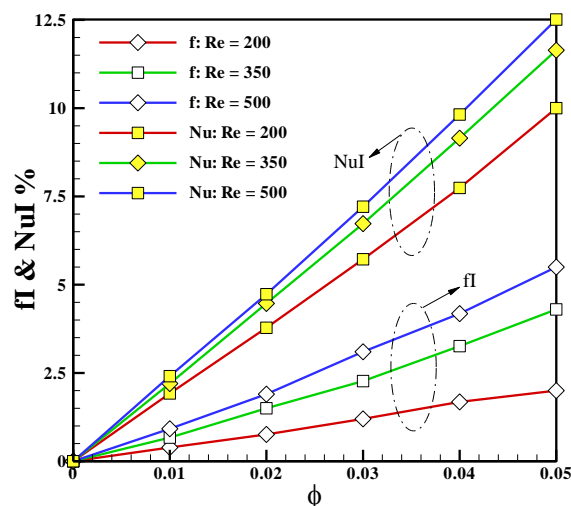


Fig. 13. Friction factor and mean Nusselt number increment for different Reynolds number vs. particle concentration.

As mentioned, in the convective heat transfer problems, the Nusselt number and the pressure drop coefficient must be considered together. As a result, based on the Reynolds analogy [20], the performance coefficient (PC), which is defined as the ratio of the Nusselt number to the friction factor for the slurry fluid to the pure fluid is introduced in Eq. (71). Then the PC is an important parameter for judging the use of the slurry fluid or not. Having $PC > 1$ in a

convective heat transfer problem means that the heat transfer characteristics are more dominant in compare with the pressure drop characteristics. Then, having $PC > 1$ is a favorable character.

$$PC = \frac{\left(\frac{Nu}{f}\right)}{\left(\frac{Nu}{f}\right)_0} \quad (71)$$

This can also be deduced from Fig. 13, which shows that the use of these microparticles does not increase the pressure drop so much, due to having a density almost equal to the density of the base fluid. The effect of the volume concentration on the PC is shown in Fig. 14 for different Reynolds number. It can be seen that, the PC for lower Reynolds number is more. Then, it's up to the designers to decide whether only heat transfer is important or whether pressure drop is important to them. But, it is clear that when this slurry is used as a working fluid in the convective heat transfer, for all states, the PC is more than one, and, it means that, convective heat transfer characteristics are more dominant in compare with the pressure drop characteristic.

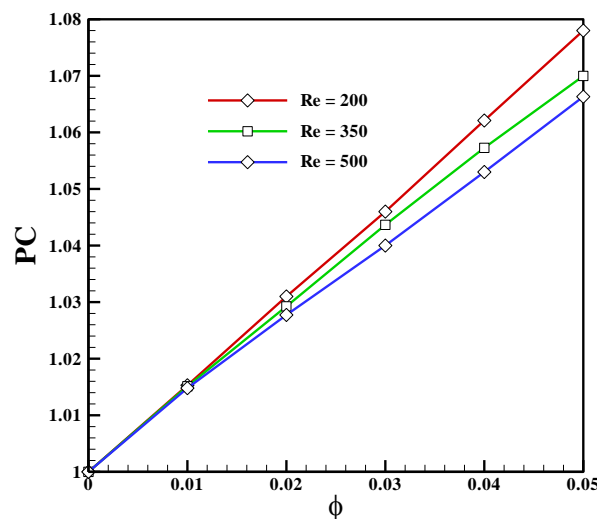


Fig. 14. Performance coefficient for different Reynolds number vs. particle concentration.

5. Conclusions

The use of microencapsulated PCMs in a base fluid, increases the convective heat transfer rate. These particles will not have a high temperature change during the phase change, and this is equivalent to having a high heat capacity. In this paper, the effect of the presence of microencapsulated paraffin with iron oxide coating in water on the heat transfer rate in the combined entrance length (hydrodynamic and thermal) in a mini-annular pipe has been investigated. The problem is solved in two phase model using the Eulerian-Lagrangian method. In this method, the fluid phase is studied by the Eulerian perspective and the particle phase is studied in the Lagrangian view. The fluid phase is also solved by a control volume method, and the SIMPLE method is used to solve the velocity and pressure fields. Due to the high Biot number for the particles, the lumped temperature assumption is not valid. Then solving energy equation in the particles is needed. In this paper, details of the energy equation solving inside each particle has been presented. The results show that the presence of particles reduces the fluid bulk temperature and increases the heat flux entering the fluid from the wall. Then, the mean Nusselt number increases, while the pressure drop doesn't increase significantly. The results show for $\phi = 0.05$ and $Re=200, 500$, the Nusselt number increases by 10 and 12.5%, while the pressure loss increases by 2 and 5.5% respectively. The maximum performance coefficient is 1.078 and occurs for $Re=200$ at $\phi = 0.05$.

References

- [1] X. Wang, J. Niu, Performance of cooled-ceiling operating with MPCM slurry, *Energy Conversion and Management*, 50 (2009), 583-591.
- [2] P.W. Griffiths, P.C. Eames, Performance of chilled ceiling panels using phase change material slurries as the heat transport medium, *Applied Thermal Engineering* 27 (2007) 1756-1760.

- [3] M. Safdari, R. Ahmadi, S. Sadeghzadeh, Numerical investigation on PCM encapsulation shape used in the passive-active battery thermal management, *Energy* (2020), doi: <https://doi.org/10.1016/j.energy.2019.116840>.
- [4] W. M. Yan, C. J. Ho, Y. T. Tseng, C. Qin, S. Rashidi, Experimental and numerical investigation of the latent heat thermal storage unit with PCM packing at the inner side of a tube, *International Journal of Heat and Mass Transfer*, 152 (2020), 119480.
- [5] M. Ghalambaz, A. J. Chamkha, D. Wen, Natural convection flow and heat transfer of nano-Encapsulated phase change Materials (NEPCMs) in a cavity, *International Journal of Heat and Mass Transfer*, 138 (2019), 738-749.
- [6] J. Rostami, A. Abbassi, J. Harting, Heat Transfer by Nanofluids in Wavy Microchannels, *Advanced Powder Technology*, 29 (4), (2018), 925-933.
- [7] M. Kalteh, A., Abbassi, M., Saffar-avval, J., Harting, Eulerian- Eulerian Two-Phase Numerical Simulation of Nanofluid Laminar Forced Convection in a Microchannel, *International Journal of Heat and Fluid Flow*, 32 (2011), 107-116.
- [8] M. Mirzaei, M. Saffar-Avval, H. Naderan, Heat Transfer Investigation of Laminar Developing Flow of Nanofluids in a Microchannel Based on Eulerian-Lagrangian Approach, *The Canadian Journal of Chemical Engineering*, 92 (2014), 1139-1149.
- [9] W. J. Minkowycz, E. M. Sparrow, J. Y. Murthy, 2006, *Handbook of Numerical Heat Transfer*, second ed., John Wiley & Sons, Hoboken, NJ.
- [10] M. Zeneli, I. Malgarinos, A. Nikolopoulos, N. Nikolopoulos, P. Grammelis, S. Karellas, E. Kakaras, Numerical simulation of a silicon-based latent heat thermal energy storage system operating at ultra-high temperatures, *Applied Energy*, 242 (2019), 837-853.
- [11] D. Wen, L. Zhang, Y. He, Flow and Migration of Nanoparticle in a Single Channel, *Heat and Mass Transfer*, 45 (2009), 1061-1067.
- [12] J. Rostami, Convective Heat Transfer by Micro-Encapsulated PCM in a mini-Duct, *International Journal of Thermal Sciences*, 161 (2021), 106737
- [13] S. V. Patankar and D.B. Spalding, A Calculation Procedure for Heat, Mass and Momentum Transfer in Three-Dimensional Parabolic Flows, *International Journal of Heat and Mass Transfer*, 15 (1972), 1787-1806.
- [14] C. M. Rhie, W.L. Chow, Numerical Study of the Turbulent Flow Past an Airfoil with Trading Edge Separation, *AIAA J.*, 21 (11) (1983) 1525-1535.
- [15] D. B. Spalding, A Novel Finite Difference Formulation for Differential Expressions Involving Both First and Second Derivatives, *International-Journal for Numerical Methods in Engineering*, 4 (1972), 551-559.
- [16] W. E. Ranz, W. R. Marshall, JR., Evaporation from Drops, *Chemical Engineering Progress*, 48 (3), (1952), 141-146
- [17] P. Bhattacharya, S. K. Saha, A. Yadav, P. E. Phelan, R. S. Prasher, Brownian dynamics simulation to determine the effective thermal conductivity of nanofluids, *Journal of Applied Physics* 95(11) (2004), 6492-6494.
- [18] W. M. Kays, M. E. Crawford, 1980, *Convection Heat and Mass Transfer*, 2nd ed., Mc Graw-Hill, New York
- [19] A. Bejan, *Convection Heat Transfer*, John Wiley& Sons, Hoboken, New Jersey, 4th ed. (2013)
- [20] J. P. Holman, in: *Heat Transfer*, eighth ed. McGraw-Hill Inc., New York (1997), pp. 218-282.
- [21] J. Y. Jung, H. S. Oh, H. Y. Kwak, Forced Convection Heat Transfer of Nanofluids in Microchannels, *International Journal of Heat and Mass Transfer*, 52 (2009), 466-472.